P1.92 TROPICAL CYCLONE FORMATION FROM THE EQUATIORIALWAVES

Chanh Q. Kieu*, Jeffrey S. Gall, William M. Frank, and Fuqing Zhang
Department of Meteorology, Pennsylvania State University, University Park, 16802

1. INTRODUCTION

It has been well-known that tropical waves play a key role in the formation of tropical cyclones (TCs). The most important characteristic of tropical waves in the TC genesis (TCG) is their persistence in providing a favorable environment for TC embryos to develop, which could account for nearly 80% of the TC genesis events in the tropical regions (Gray 1968; Ritchie and Holland 1997; Zehnder et al. 1999; Molinari et al. 2000; Dickinson and Molinari 2002; Frank and Roundy 2006; Dunkerton et al. 2009; Fang and Zhang 2010). There are numerous studies of TC genesis associated with tropical waves, but the existence of various types of waves including the equatorial Rossby waves, the easterly waves of the Atlantic, the equatorial Kelvin waves, and mixed Rossby-gravity waves, as well as their strong interactions with the environment render the problems of predicting and understanding TCG processes challenging (Frank and Roundy 2007). The essential issue with the TC research is that there are abundant disturbances associated with tropical waves that satisfy the necessary conditions for the TCG to occur, but only small fraction of these disturbances could actually grow into TCs (e.g., Gray 1968; Avila and Pasch 1992; Harr and Elsberry 1996; Simpson et al. 1997; Wang and Magnudosttir 2005) .

In recent investigations of the TCG associated with easterly waves, Montgomery et al. (2009) and Dunkerton et al. (2009) showed that the crucial condition for tracking the TCG in the Atlantic basin lies in our capability to indentify a critical vertical layer in which the phase speed of the waves with respect to the mean flows is zero. Such a layer, which is often accompanied by the largest difference between streamfunction and streamline, can be used as a criterion to distinguish between non-developing versus developing vorticity centers. Dunkerton et al. (2009) revealed that a large number of the genesis cases are connected with these hot spots during the 1995-2001 hurricane seasons, which give us a potential capability to predict TCG in future. The existence of such hot spots has been however long recognized as one of the necessary requirements for the TCG to occur, which is often re-phrased in terms of initial tropical disturbances (e.g., Gray 1968, 1975; Yanai 1968; Challa and Pfeffer 1990; Zehnder et al 1999; DeMaria et al 2001). These disturbances are of course not sufficient as several other criteria should be taken into account as well including sea-surface temperature (SST), vertical wind shear, vertical instability, and midlevel moisture variables. The ability to predict the TCG associated with such tropical disturbances is of major importance, and has been a long haul in the TCG research to date.

Gall et al. (2009, hereinafter referred to as G09) and Gall and Frank (2009) provided a thorough examination of the TC genesis associated with one specific class of tropical waves, the easterly equatorial Rossby (ER) waves. Their idealized experiments shed some clues into the formations of TCs in which the amplitude of waves is identified as the main criterion for the TCG in a resting background environment. In a sheared environment, they have demonstrated that non-developing disturbances could interact with the background flows and develop fully into TCs within a reasonable time scale. In this study we will extend further the work by G09 by focusing on various intermediate wave projections during the TCG and the roles of the small-scale deep convection to the class of non-developing disturbances classified in G09. Recent studies, e.g., by Hendricks et al (2004) and Montgomery et al (2006) have provided some evidence about the roles of the deep convection in the TCG processes, and it is thus of importance to examine the relative roles of these convective scale processes as compared to the tropical wave amplitude in the TCG. Furthermore, it remains uncertain how the equatorial Rossby waves could evolve directly into initial disturbances and how they could trigger some other types of equatorial waves, whose interactions are not well understood.

The next section provides a brief description of our idealized experiment and initialization. Section 3 describes the projection of the ER waves onto the equatorial Kelvin waves and how the interaction of the ER and Kelvin waves lead to a series of TCG events. Section 4 shows in detail the early characteristics of one TCG event that is captured in our cloud-resolving simulation. Section 5 presents the budget calculations of the vorticity and divergence equations. Concluding remarks are given in the final section.

2. EXPERIMENTAL DESIGN

This study uses the Weather Research and Forecasting (WRF) model Version 3.1 (Skamarock et al. 2005). The model setups and configurations are similar to those in G09 including 31 vertical levels, a six-species cloud microphysics package (Lin et al. 1983), the modified version of the Kain- Fritsch scheme (Kain and Fritsch 1993), the Yonsei University (YSU) scheme atmospheric boundary layer is parameterized using (Hong and Pan 1996), and the Monin-Obukhov surface layer scheme is used to compute the surface exchange coefficients for heat, moisture, and momentum. Several key differences from G09's model setup are 1) the outermost domain size in the east-west direction is reduced from 10

* *Corresponding author*: Dr. Chanh Kieu, Lab of Climate and Weather Research, Hanoi College of Science, Vietnam National University, Hanoi, Vietnam 10000. email: kieucq@atmos.umd.edu.

wavelengths to a smaller size of 2 wavelengths such that the horizontal grid spacing can be reduced homogeneously from 81 km as in G09 to 9 km in our experiments over the entire domain; 2) a two-way nested domain of 601 x 601 horizontal grid points with 3-km grid spacing is introduced about 3 days before a genesis event occur to capture the details of the TC genesis at the cloud-resolving (convection-permitting) resolution. The nested domain is centered at one of the ridges of the initial ER waves where a TC genesis event is known to occur from a previous 9-km-only coarser-resolution run, and it is set to move with the storm automatically once the disturbance reaches the tropical depression strength, and 3) the initial wave amplitude is set equal to 0.16, which corresponds to the non-genesis classification in G09's study.

The model initialization is designed with two idealized configurations: one with a tropical strip of the equatorial Rossby waves exactly the same as in G09, and the other with a strip of the equatorial Kelvin waves. The horizontal structure of the meridional mode number one (n = 1) equatorial Rossby (ER) wave is given according to the shallow water theory, while the Kelvin wave initialization is taken from the simplified shallow water model whose perturbation geopotential and horizontal flows are given by (see, e.g., Holton 2004):

$$
\begin{aligned}
u(x,y) &= U_0 e^{-\beta y^2/2c}, \\
v(x,y) &= 0, \qquad\qquad (1) \\
\phi(x,y) &= cU_0 e^{-\beta y^2/2c},
\end{aligned}
$$

where c is the phase speed of the waves that is determined by the equivalent depth of the model, β represents the variation of the Coriolis parameter in the meridional direction, y is distance from the equator, and U_0 is an initial wave amplitude. In our experiment, U_0 is chosen to be 8 m^{-1} such that the wave amplitude corresponds to the nondimensional value of 0.16 as in G09. For the vertical structure of both ER and Kelvin waves, a vertical profile $G(z)$ is taken from Wheeler (2002), which provides a simple relationship between the vertical wavelength of a particular normal mode in a constant stratification atmosphere and its equivalent depth. This function $G(z)$ is applied simultaneously to both the wind and mass fields in our both ER and Kelvin wave initializations. To ensure also the balance requirement of the perturbation, the perturbation temperature is derived from the geopotential perturbation. The moisture and background temperature fields are assumed to follow the Jordan (1958)'s mean hurricane season sounding. By vertically integrating the hydrostatic equation and using the Jordan sounding, a hydrostatic base state pressure profile is calculated. Note that because the initial base state winds are zero, the entire meridional and zonal structure is given by the ER wave perturbation winds. As mentioned in G09, although the initial condition may not be exactly in "model balance", our initialization represents a good first guess for such a balance as evidenced by the lack of gravity wave noise in the earlier period of simulations.

3. KELVIN WAVE PROJECTION

Figure 1 shows the time series of the sea level pressure anomaly, which is defined as the difference between the total sea level pressure and the area-averaged value over the entire domain, and surface wind during the first 2 days of integration. Except for the first 12 hours of the model integration during which the model state is adjusting to the new

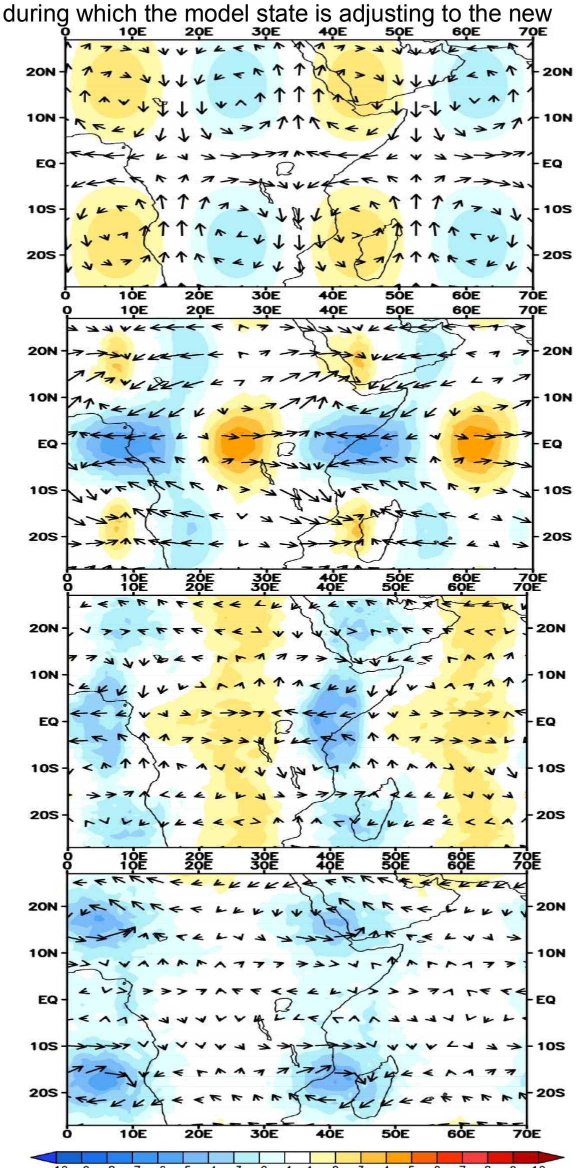

Figure 1. Time series of the horizontal cross sections of sea level pressure anomaly (shaded, unit 1 hPa), superimposed with surface wind during the first 4 days of interaction valid at a) t = 0 h, b) t = 12 h, c) t = 48 h, and d) t = 96 h.

balance governed by the model constraints, one can see that the initial ER waves distort quickly and project into the equatorial Kelvin wave mode (in this study, the signal of the Kelvin wave signal is identified in terms of typical patterns of low (high) centers together with corresponding convergence (divergence) distributions along the equator). After t = 12 h, two Kelvin waves with the wavelengths similar to those of the ER waves become well enough defined and so dominant that the ER wave signal seems to disappear entirely. The alternative evolution of the ER and Kelvin waves reveals a quite distinct nature; either the ER waves or the Kelvin waves are dominant at any instant of time. The persistent eastward propagation of the Kelvin waves, which is one of the key characteristics of the Kelvin waves that distinguishes them from the other types of equatorial waves, can be seen evidently during the first 5 days of integration not only at the surface but also up to 700 hPa level. It should be noted that although the influence of the Kelvin waves tends to decrease with latitude (see Eq. (1)), the meridional scale of the ER waves is actually wide enough that it results in an intermediate zone between 10^0 - 18^0N where mutual interactions between the two types of waves favor the generation of tropical disturbances as will be seen below and in more detail in Section 4. Note also that due to the artificial vertical profile *G*(*z*), both Kelvin and ER waves are travelling at different speeds at different levels.

To understand more quantitatively the projection of the ER waves onto Kelvin waves, we note again from the dispersion relationship of the equatorial mixed Rossby–gravity waves that the wave projection tends to be most effective at the long wave regimes, given an initial wavelength of the ER waves. The optimum threshold for the projection takes place within the very large wavelength limit and the wavelength at which the wave frequency is peaked. Within the shorter wavelength regime, the projection to Kelvin wave will require very high temporal frequencies that tend to decay rapidly, and therefore have no significant impacts on the large-scale interaction (T. Dunkerton, personal communication). To calculate explicitly the wave number k_m below which the wave projection is most effective, we start from the mixed Rossby-gravity dispersion relation (see, e.g., Holton 2004)

$$\frac{c}{\beta}\left(-\frac{k}{\omega}-k^2+\frac{\omega^2}{c^2}\right)=2n+1\,. \quad (2)$$

At the long-wave limit of $k \to 0$, ω is small enough such that the term ω^2/c^2 will be assumed to be much smaller than the first two terms on the lhs of Eq. (2). Under this approximation, we obtain:

$$\omega \approx -\frac{k\beta c}{(2n+1)\beta + k^2 c}\,. \quad (3)$$

This approximated dispersion relationship for the long wave limit will take the maximum value ω_m at k_m given by:

$$k_m = \left(\frac{(2n+1)\beta}{c}\right)^{1/2}, \quad (4)$$

from which

$$\omega_m = \frac{1}{2}\left(\frac{\beta c}{(2n+1)}\right)^{1/2}. \quad (5)$$

A quick check of these values will confirm that our approximation of neglecting ω^2/c^2 as compared to the other terms on the lhs of Eq. (2) is reasonable. For all of our experiments in which the equivalent depth *H* is set to 3×10^3 m, k_m will be roughly 4.1×10^{-7} m^{-1} for the *n* = 1 ER waves, which corresponds to a wave length of 1800 km. Because the critical wave number k_m will be larger for the smaller equivalent depth, the wave projection is expected to be more competent in the lower troposphere once the initial waves possess sufficient long wavelengths. Since we impose an initial wavelength of ~ 4500 km, this indicates that our initialization of the ER waves is well in the favorable regime for the projection to occur throughout the lower troposphere.

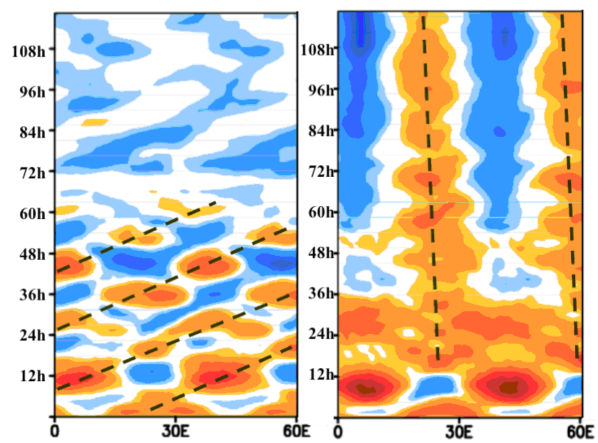

Figure 2. Hovmoller diagram of sea level pressure during the first 5 days of integration for Kelvin waves at the Equator (left panel) and easterly Rossby waves at 20^0N (right panel).

Of importance is that the projected Kelvin waves propagate eastward at much faster pace than the westward propagation of the ER waves, especially in the lower troposphere where the projection is most apparent. The Hovmoller diagram of the sea level pressure in Fig. 2 shows that the ER waves propagate roughly at the speed of 3 m s^{-1} as also seen in G09's experiment, whereas the Kelvin waves propagate at about 25 m s^{-1}, which corresponds to an equivalent depth of approximately 65 m. Such shallow characteristics of the projected Kelvin waves will be seen later to be a potentially important condition for the interaction of the Kelvin and ER waves that leads to a series of TCG events. It should be mentioned that, unlike the n = 1 ER wave for which the propagation speed depends not only on the equivalent depth but also on the normal mode *n*, the beta effect as well as the wave number, the Kelvin waves are non-dispersive with the propagation speed depending on only the equivalent depth. Given the same wavelength near the low *k* spectrum, the Kelvin waves are supposed to travel with a faster speed than the n = 1 ER waves, which can be seen in Fig. 2. It is worth noting further that the above wave propagation does not seem to depend on the resolution or the size of the model domain. Our tests of 10-wave length domain as in G09 or simple use of 81 km resolution all yield similar wave projection and propagation.

After 3 days of integration, a string of low pressure systems start to show up near the southern and northern tips of the Kelvin waves (~ 20^0N and 20^0S), and the Kelvin waves appear to weaken rapidly afterward. That the TCG is taking place near the zone where both Kelvin and ER waves are interfering suggests that the interactions between these two types of waves could play some role in the formation of the initial disturbances that result in genesis. Although the signal of the Kelvin waves still exists after the genesis occurs, the ER waves do not appear to support further the development of the Kelvin wave excitation. As a result, the Kelvin wave amplitude attenuates with time.

To isolate the importance of the interaction of the ER waves and Kelvin waves in the TCG, we perform an additional experiment in which we initialize the model with the pure Kelvin waves. It is interesting to note that these pure Kelvin waves do not project into ER waves but simply dissipate with time, and there is no wave interaction as in the ER experiment (not shown). Such ineffectiveness of the projection from the Kelvin waves onto the ER waves could be attributed to the distribution of the Kelvin wave energy, which concentrates mostly along the equator. For the ER waves, the total kinetic energy spreads symmetrically along the pressure centers, which cover a wide strip from 35^0S to 35^0N. This allows part of the ER wave energy to project onto the Kelvin waves as opposed to the local energy distribution of the Kelvin waves. After 3 days of integration, the Kelvin wave signals become so weak that no significant tropical disturbances appear. Such trivial roles of the Kelvin waves appear to be consistent with the observational study of Frank and Roundy (2006), which indicates that Kelvin waves is of no significance in providing potential initial disturbances for the TC genesis.

In the next, we will focus only on the genesis phase, which is between 108 and 132 h of model integration as shown in Fig. 3. The main goal here is to understand what favorable conditions that the tropical waves provide for the perturbations to develop and how the perturbations intensify.

4. CYCLOGENESIS

As seen in Fig. 1, the string of low pressure centers that develop around 3 days into integration are fairly stable for about 1 day, but they begin to experience a rapid intensification after t = 136 h. Within a period of 18 hours, the systems reach hurricane intensity with the maximum surface winds of 31 m s^{-1} and a minimum sea-level pressure of 984 hPa as seen in Fig. 3. Under the influence of beta-drifting, all of the lows in the northern (southern) hemisphere move further north (south) and maintain their hurricane intensity for another 12 hours. While the disturbances can also be seen at t = 72 h from the 9-km domain without the nested domain, simple experiments of using a single 9-km domain reveals that the subsequent intensification of these disturbances does not occur, similar to the conclusion documented in G09 (not shown). Thus, the above rapid intensification of the initial disturbances is strictly associated with the 3-km nested domain, even though this nested domain is activated about 2 days before the intensification happens. This implies that the small-scale convective processes resolved by the 3-km domain must have contributed favorably for the intensification that we would like to focus on in more detail. There are two different processes that should be highlighted here; one associated with the larger-scale pre-conditioning for the TCG by the tropical waves, and the other is the small-scale convection.

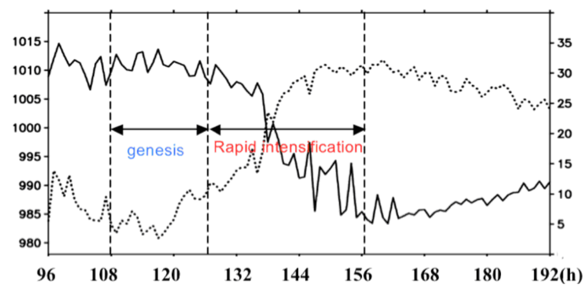

Figure 3. Time series of the evolution of the minimum sea level pressure (solid, unit hPa) and maximal surface wind (dotted, unit m s^{-1}) of the TCs within the nested domain.

To look more deeply into the roles of small-scale deep convection on the early genesis phase, Figure 3 shows the time series of vertical cross sections of the tangential flows through the storm center captured in the 3-km resolution nest about 2 days before the rapid intensification occurs. This storm center exhibits an ensemble of local strong vertical motions with scales of 10-20 km. The low-pressure systems associated with the early disturbances are initially characterized by a midlevel cyclonic flow of the size ~ 500 km as well as a dry core at midlevels (not shown). These strong pulses of vertical motions are consistent with pools of strong low level convergence (LLC) associated with the shallow characteristics of the projected Kelvin waves discussed in section 3. Of interest is that such regions of LLC are located right beneath the midlevel cyclone, and are observed only after t = 120 h. As soon as this LLC is aligned vertically with the midlevel cyclone, it is seen from the subsequent evolution of the tangential flows that the system starts to build up rapidly, starting first near in the lower levels (Fig. 4). This is expected as it indicates the roles of the angular momentum conservation (or more directly, the stretching term in the vorticity budget equation that will be discussed in the next section). The core of the system also moistens rapidly with the relative humidity approaching 100% from the surface up to the 15 km. In the recent study by Nolan (2008), the moistening of the midlevels is believed to be a criterion for the TC genesis to occur, but it is seen in our experiment that such moistening is more like a consequence of the low-level convergence, which brings moist air from the boundary up to higher levels. While the phase lock of the low-level convergence line associated with the Kelvin wave and the midlevel

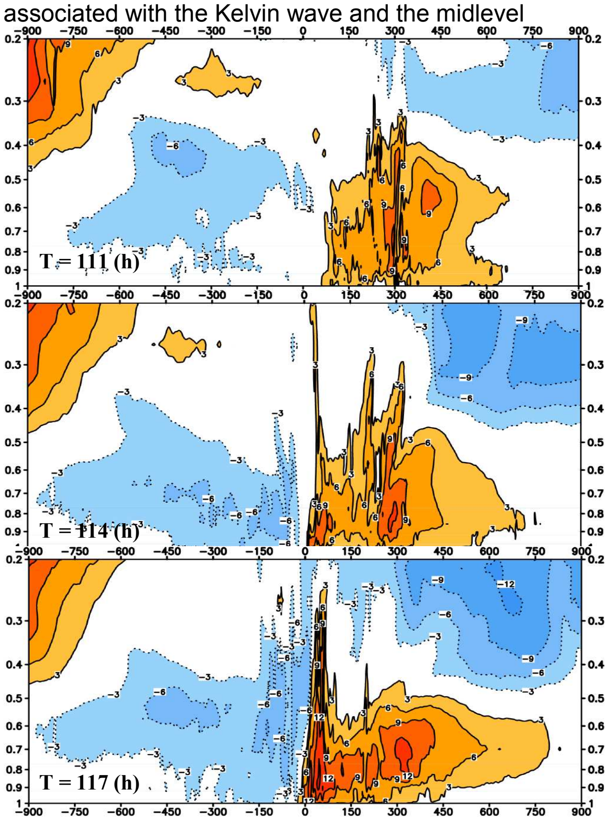

Figure 4. Evolution of the east-west vertical cross section of the tangential wind (contoured at intervals of 3 m s^{-1}) through the center of the disturbance during the rapid intensification period from t = 111 h to t = 120 h.

cyclonic flows associated with the ER waves gives rise to favorable initial disturbances, it is the strong interaction between the low-level convergence, which is enhanced by the high-resolution nested domain, and the midlevel vortex that leads to the intensification of the disturbances. Viewed from this perspective, the small-scale deep convection is more a manifestation of the enhanced LLC rather than a process that is driving directly the bottom-up development of the disturbances. The work of Dunkerton et al. (2009) suggests that the hot spots for the TCG are the location where the vorticity center and divergence center are coincident. What we notice here however is a more specific situation; the vorticity centers can actually be located in the midlevels with the LLC centers below. They do not need to be at the same level for the *translating gyre*[1] to be protective. In this sense, a vorticity center does not need to be a pouch to grow; the vorticity center could potentially develop as soon as a lower level convergence associated some other types of tropical waves (such as Kelvin waves in our case) could propagate and align beneath the vorticity center. After the low-level circulation attains the depression threshold, the wind-induced surface heat exchange feedback (Emanuel 1988) could be the main explanation of why the system rapidly intensifies.

5. BUDGET CALCULATION

As discussed in section 3, the vertical alignment of the lower level convergence and the midlevel vorticity is believed to be the critical condition for the rapid intensification to occur. To see how such an occurrence of the LLC beneath a midlevel vorticity could lead to the spinup of the disturbances in a more quantitative manner, budget calculations for the vorticity and divergence equations are performed in this section. Under balance dynamics, it should be recalled that the divergence equation is often simplified as a balanced equation whose combination with the hydrostatic equation could serve as a constraint in various balanced models. For the study of the TCG problem, particularly at the early phase where a close circulation at the surface is not well defined, the gradient balanced assumption is of course not ensured. Our purpose here is to examine how the lower level convergence and midlevel vorticity can nurture each other in a favorable way for the system to develop.

To this end, we formulate the vorticity equation in the flux form as follows (see Haynes and McIntyre 1987)

$$\begin{aligned}\frac{\partial \eta}{\partial t} &= -\frac{\partial}{\partial x}\left(u\eta + w\frac{\partial v}{\partial z} - F_y\right) - \frac{\partial}{\partial y}\left(v\eta - \frac{\partial u}{\partial z} + F_x\right) + SOL \\ &= -\left[\frac{\partial (u\eta)}{\partial x} + \frac{\partial (v\eta)}{\partial y}\right] - \left[\frac{\partial}{\partial x}\left(w\frac{\partial v}{\partial z}\right) - \frac{\partial}{\partial y}\left(w\frac{\partial u}{\partial z}\right)\right] + \left[\frac{\partial F_y}{\partial x} - \frac{\partial F_x}{\partial y}\right] + SOL \qquad (6)\end{aligned}$$

where the rhs terms of Eq. (6), upon taking an area integration, represent the flux divergence of vorticity forcing through the lateral boundaries, the divergence of vertically tilted horizontal vorticity, frictional and solenoidal contributions to the rates of changes of the absolute circulation over the control area, respectively. In our calculation, a control column of the size 1200 km x 1200 km x 12 km following the disturbance's center is chosen for all of budget calculations. Because the last rhs term in (6) appears to be much smaller than the first three terms, it will be ignored for the purpose of our vorticity budget analysis.

For the divergence budget equation there exists no close divergent form and we therefore express the local tendency in the form as:

[1] *Translating closed gyre* discussed in Dunkerton et al (2009) refers to a protected region that can be identified by viewing a tropical wave critical layer in a frame of reference moving at the phase speed of the wave. As suggested in Dunkerton et al (2009), such gyre is often accompanied by a vortex that may subsequently grow to a tropical depression-strength vortex.

$$\frac{\partial D}{\partial t}=-\alpha\nabla^2 p-D^2+2J(u,v)-\beta u+f\xi-\left(\frac{\partial w}{\partial x}\frac{\partial u}{\partial z}+\frac{\partial w}{\partial y}\frac{\partial v}{\partial z}\right)-\left(\frac{\partial \alpha}{\partial x}\frac{\partial p}{\partial x}+\frac{\partial \alpha}{\partial y}\frac{\partial p}{\partial y}\right)$$
$$+\left(\frac{\partial F_x}{\partial x}+\frac{\partial F_y}{\partial y}\right)-\vec{V}\bullet\nabla D \tag{7}$$

where $\alpha=1/\rho$ is the specific volume, and $D=\frac{\partial u}{\partial x}+\frac{\partial v}{\partial y}$ is the horizontal divergence. The terms on the rhs of Eq. (7), respectively, represent (1) the convergence induced by the horizontal Laplacian of the pressure, (2) the destructive effects of the divergence caused by its own convergence, (3) the Jacobian effect, (4) the beta effect, (5) the vorticity forcing, (6) the tilting effect similar to the tilting of the vorticity budget equation, (7) the solenoidal term similar to that on the vorticity budget equation, (8) the frictional effect, and (9) the advective effect.

Of all terms, the first, second, and the fifth terms on the rhs of Eq. (7) are of most significance to the generation of the low level convergence. Physically, the first term (hereafter PLAP) represents the convergence induced by a low pressure center. The lower the pressure is at the center of the disturbance, the stronger the convergence will be. For the second term (hereafter DIVS), its physical meaning can be revealed if one notices that the large horizontal convergence will tend to produce a stiffer core, which decelerates the converging inflows more effectively and thus results in stronger convergence. Regarding the fifth term on the rhs of Eq. (7) (hereafter VORF), this is the term that exhibits most directly the roles of the relative vorticity in controlling the rate of convergence generation, much like the stretching forcing in the vorticity budget equation (the first term on the rhs of Eq. 6). This VORF term implies that the strong relative vorticity, or equivalently the strong horizontal shear, will induce a large difference in the Coriolis acceleration of the horizontal winds, causing more divergence. Although the DIVS and VORF terms are often opposite in sign for cyclonic convergent flows in most practical patterns, the explicit expression of the relative vorticity to the convergence budget in Eq. (7) allows us to examine the mutual interaction of the relativity vorticity and convergence in a clear manner. Because of the dominant roles of these above three forcing terms in generating the horizontal convergence, we will henceforth group the contributions of other term including Jacobian, “tilting”, “solenoidal”, and advection terms into a single variable to ease our subsequent discussions.

The height-time cross sections of the control-area averaged vorticity η and the corresponding forcings on the rhs of Eq. (6) exhibit a strong signal of the vorticity generation near the surface during the genesis phase. The development of the surface vorticity is in agreement with the evolution of the tangential flows seen in Fig. 4 including the midlevel characteristics from t = 96 h to t = 120 h, and a low level spinup between t = 120-144 h into integration. As expected, the stretching term shows a maximum forcing at the lowest levels where the LLC is most significant, whereas the tilting term has negligible contribution to the vorticity budget. We notice, however, that all resulting cyclones developed from our tropical wave experiments, even at their peaked intensity, have a fairly shallow depth of cyclonic flow, which occupies mostly the lower half of the troposphere up to z = 7 km (see also Fig. 4). Such shallow characteristic of the vortex could be attributed to our use of the vertical profile $G(z)$ discussed in Section 2. This external function represents a particular normal mode that imposes a strong anti-cyclonic background flow at the upper half of the troposphere and acts as a lid preventing the penetration of the vortex. This is seen clearly after t = 156 h with a broad layer of anti-cyclonic flow aloft. As a result, the area-averaged cyclonic flow concentrates mostly below z = 7 km.

Of importance is that the LLC associated with the Kelvin waves grows rapidly after it moves underneath the midlevel vorticity. Between t = 108 and 120 h, the low pressure center associated with the existing midlevel disturbance is rather weak, and PLAP does not have any significant contribution to the enhancement of the LLC (Fig. 5). Similarly, the VORF term has minimum impacts near the surface but largest amplitude at the midlevel where the relative vorticity is peak near the melting level. Unlike other forcings, DIVS is always negative and concentrates mainly near the top of the boundary where convergence is usually maximized. It should be mentioned that before the alignment of the LLC and midlevel vortex occurs, the divergence balance is mostly among the Jacobian, DIVS, PLAP, and VORF forcing terms, which are commonly expressed in terms of the balanced equation (e.g., Holton 2004). However, as soon as the LLC approaches the background rotational environment associated with the midlevel disturbance, such quasi-balance will no longer be maintained, and DIVS shows an explosive amplification, leading to an enhancement of both the low level circulation and the LLC (Fig. 5). Note here two dual roles of the enhanced surface circulation. On one hand, it will reduce the LLC as controlled by the VORF term. On the other hand, it will help increase the surface fluxes, which results in larger diabatic heating and thus deepens the sea surface pressure. That both PLAP and DIVS show an increase in magnitude indicates that the thermodynamic roles of the enhanced surface circulation are more significant.

As the system starts to grow after t = 144 h, the pressure at the lowest levels deepens, thus increasing the magnitude of PLAP at a faster rate. The resulting system thus evolves rapidly with time with the relative vorticity spinning up gradually from the bottom up. The mutual growth of both vorticity and divergence is therefore cooperating for the subsequent rapid intensification as seen in Fig. 3. A careful examination of LLC cross sections (not shown) reveals further that the LLC amplification takes place about 12 h prior to the low level spinup of the surface circulation, which indicate that the LLC associated with the projected Kelvin waves is likely to be the cause of the low level vorticity generation. In this regard, we believe that the key condition for the rapid intensification of a tropical disturbance lies in the vertical arrangement of the LLC and midlevel disturbances.

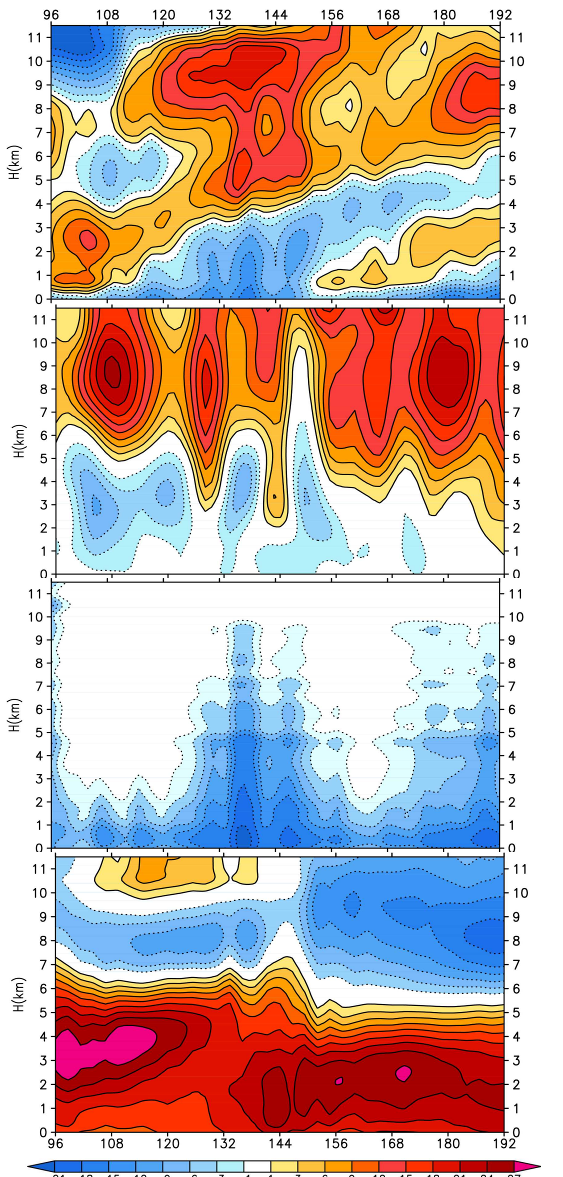

Figure 5. Height-time cross sections of the divergence budget calculation for (700 km × 700 km) area-averaged quantities from the model outputs: (a) 2D convergence (every 2×10^{-5} s^{-1}), (b) Laplacian of the pressure perturbation; (c) vorticity term; and (d) divergence squared term. The solid/dashed contours are for the positive/negative values.

6. CONCLUSION

In this study, we have extended further the work by G09 to examine the different interactions of tropical waves in tropical cyclogenesis, and the subsequent rapid intensification at the convective scales. Idealized experiments with the equatorial Rossby waves initialization have shown that the pure equatorial Rossby waves do not evolve directly into incipient TC embryos but project first onto the Kevin equatorial wave modes. The projection is most effective at the lowest levels where the spectrum of projected Kelvin waves could accept a wide range of wave length from very long planetary wave to a wave with wavelength as short as 1800 km. The shallow characteristics of the projected Kelvin result in intriguing interaction with the equatorial Rossby waves in which the low level convergence associated with the eastward Kelvin waves could align with the middle level disturbances associated with the equatorial Rossby waves. Such vertical alignment of these two types of waves gives rise to a string of the initial disturbances from which cyclogenesis events could be triggered. A further experiment of the pure Kelvin wave initialization has demonstrated also that the Kelvin waves alone are however not as effective as the equatorial Rossby waves in triggering the TC genesis. The projection of the Kelvin waves back to the equatorial Rossby waves does not occur, and thus there is no interaction between waves. As a result, no cyclogenesis events have been observed from the pure Kelvin wave initialization experiment. This is consistent with previous studies that the Kelvin waves and their associated westerly wind bursts are not as effective a mechanism for the tropical cyclogenesis as are other types of tropical waves.

While the initial projection of the ER waves into the Kelvin waves and their subsequent interaction could generate a number of disturbances that are favorable for the development of TCs, such disturbances could not intensify without sufficient low level convergence. By increasing the resolution of the simulations up to the cloud-resolving resolution, the low level convergence is enhanced substantially and all non-developing cases in G10's experiments could grow into TCs. The strengthened lower level convergence manifested itself as a collection of deep convective towers, thus revealing the important roles of the deep convection in the TC genesis. Our budget calculations have shown an explosive development of the low level convergence and surface generation of cyclonic circulation after the low level convergence associated with the projected Kelvin waves located beneath the midlevel disturbances. The enhancement of the low level convergence can be seen from multiple pulses of deep convection at the cloud-resolving scales. This indicates that deep convection is an important component that could actually help spin up the disturbances during the rapid intensification of TCs.

REFERENCES

Avila, L.A., and R.J. Pasch, 1992: Atlantic tropical systems of 1991. *Mon. Wea. Rev.*, **120**, 2688–2696.

Black, M.L., J.F. Gamache, F.D. Marks, C.E. Samsury, and H.E. Willoughby, 2002: Eastern Pacific Hurricanes Jimena of 1991 and Olivia of 1994: The effect of vertical shear on structure and intensity. *Mon. Wea. Rev.*, **130**, 2291–2312.

Challa, M., and R. L. Pfeffer, 1990: Formation of Atlantic hurricanes from cloud clusters and depressions. *J. Atmos. Sci.,* **47**, 909-927.

DeMaria, M., 1996: The effect of vertical shear on tropical cyclone intensity change. *J. Atmos. Sci.,* **53,** 2076-2087.

DeMaria, M., J. A. Knaff, and B. H. Connell, 2001: A tropical cyclone genesis parameter for the tropical Atlantic. *Wea. Forecasting*, **16**, 219–233.

Dickinson, M., and J. Molinari, 2002: Mixed Rossby–gravity waves and Western Pacific tropical cyclogenesis. Part I: Synoptic evolution. *J. Atmos. Sci.*, **59**, 2183–2196.

Emanuel, K. A., 1986: An air-sea interaction theory for tropical cyclone. Part I: Steady state maintenance. *J. Atmos. Sci*., 4**3**, 585-604.

Fang, J and F. Zhang, 2010: Initial development and genesis of Hurricane Dolly (2008). *J. Atmos. Sci.*, **63**, 655-672.

Frank, W. M., and P. E. Roundy, 2006: The role of tropical waves in tropical cyclogenesis. *Mon. Wea. Rev.*, **134**, 2397–2417.

Fritsch, J.M., J.D. Murphy, and J.S. Kain, 1994: Warm core vortex amplification over land. *J. Atmos. Sci.*, **51**, 1780–1807.

Gall J. S., Frank W. M., and Wheeler M. C. (2009) The role of equatorial Rossby waves in tropical cyclogenesis Part I: Idealized numerical simulations in an initially quiescent background environment. *Mon. Wea. Rev.,* In Press.

_____., and Frank W. M. (2009) The role of equatorial Rossby waves in tropical cyclogenesis Part II: Idealized simulations in a monsoon trough environment. *Mon. Wea. Rev.,* In Press.

Gray, W. M., 1968: Global view of tropical disturbances and storms. *Mon. Wea. Rev.,* **96**, 669-700.

Kain, J. S., and J. M. Fritsch, 1990: A one-dimensional entraining/detraining plume model and its application in convective parameterization. *J. Atmos. Sci.*, **47**, 2784-2802.

McBride, J. L, and R. Zehr, 1981: Observational analysis of tropical cyclone formation. Part II: Non-developing versus developing systems. *J. Atmos. Sci*., **38**, 1132-1151.

Mlawer, E. J., S. J. Taubman, P. D. Brown, M. J. Iacono, and S. A. Clough, 1997: Radiative transfer for inhomogeneous atmosphere: RRTM, a validated correlated-k model for the long-wave. *J. Geophys. Res.*, **102**, 16663-16682.

Molinari, J, D. Vollaro, David, S. Skubis, and M. Dickinson, 2000: Origins and mechanisms of Eastern Pacific tropical cyclogenesis: A case study. *Mon. Wea. Rev.,* **128**, 125-139.

_____, D. Knight, M. Dickinson, D. Vollaro, and S. Skubis, 1997; Potential vorticity, easterly waves, and Eastern Pacific tropical cyclogenesis. *Mon. Wea. Rev.,* **125**, 2699–2708.

Skamarock, W. C., J.B. Klemp, J. Dudhia, D. O. Gill, D. M. Barker, W. Wang, and J. G. Powers, 2005: A Description of the advanced research WRF Version 2, *NCAR Technical Note*, 100p.

Wheeler, M. C., 2002: Tropical meteorology: Equatorial waves. In: J. Holton, J. Curry, and J. Pyle (eds), *Encyclopedia of Atmospheric Sciences*. Academic Press, pages 2313–2325.

Zehnder, J.A., D.M. Powell, and D.L. Ropp, 1999: The interaction of easterly waves, orography, and the intertropical convergence zone in the genesis of eastern Pacific tropical cyclones. *Mon. Wea. Rev.*, **127**, 1566–1585.